Proceedings of the 21st ICSMGE, Vienna, Austria, 14 – 19 June 2026. Pistrol, Adam & Schweiger (eds.)
Published by: ÖGG, Austrian Society for Geomechanics, Salzburg, Austria, ISBN 978-3-9503898-4-5
https://doi.org/10.53243/ICSMGE2026-1611

Determination of the variable contact geometry between a vibrating drum and the soil surface from measurements

Johannes Pistrol, Mario Hager
Institute of Geotechnics, TU Wien, Austria, johannes.pistrol@tuwien.ac.at

ABSTRACT: The paper presents a geometric model for the determination of the variable contact geometry between the drum of a vibratory roller and the soil surface from measurements. The main non-linearities of the dynamic roller-soil interaction are the continuously varying contact conditions and geometry between the drum and the subgrade as well as the curved drum geometry. As the drum penetrates the soil during the loading phase, the contact area between the two contact partners increases, which in turn affects the resulting soil reaction force and influences the motion behavior of the drum at the same time. Moreover, a periodic loss of contact between drum and soil during the unloading phase usually occurs, and the two subsystems move separately and independently from each other for a short period of time. The model introduced in the paper allows for a calculation of the variable contact geometry based on horizontal and vertical accelerations, measured in the bearing of the vibrating drum. The model is tested on measurements conducted with a typical single-drum roller. The presented findings allow for a more accurate consideration of the actual contact conditions between the drum of a vibratory roller and the soil and are considered valuable for the further development of measurement values of Intelligent Compaction.

KEYWORDS: Roller compaction, soil dynamics, intelligent compaction.

1 INTRODUCTION

Vibrating rollers are the primary tool for near-surface compaction in earthworks. A vibratory roller uses a rotating-mass type of excitation in the axis of the drum to induce a predominantly vertical load transfer into the soil. The dynamically excited drum and the underlying soil form an oscillating interaction system with changing contact conditions. Different modes of operation of the interaction system may be observed, depending on the tuning of roller design parameters, process parameters, and soil stiffness (Adam, 1996).

The characteristics of the motion behavior of the vibrating drum can be used to assess the compaction state of the soil or its load-bearing capacity. This basic idea has been used for decades by systems for Continuous Compaction Control (CCC) and Intelligent Compaction (IC) (Thurner and Sandström, 1980; Adam, 1996; Kopf, 1998; Anderegg and Kaufmann, 2004; Mooney and Rinehart, 2009).

In 1979, Thurner and Sandström (1980) found that the motion behavior of a vibrating drum depends on the stiffness of the soil. They used this finding to introduce the first system for CCC with vibrating rollers which enables a work- and roller-integrated monitoring of the compaction process. Since then, numerous research studies have been conducted to better understand the interaction between the vibrating drum of a vibratory roller and the soil (Yoo and Selig, 1979; Anderegg and Kaufmann, 2004).

The mechanics of the drum-soil interaction have for example been modeled by means of lumped parameter models (Yoo and Selig, 1979; van Susante and Mooney, 2008) or cone models (Adam, 1996; Kopf, 1998). All these studies assume a constant contact geometry between the drum and the soil.

In more recent research, dynamic elasto-plastic finite element models have been developed (e.g. Cao et al., 2011) to investigate the interaction between a vibrating drum and the soil. Kenneally et al. (2015) already highlight the importance of the consideration of the variable contact geometry between the drum and soil in their FE analysis.

A most recent study (Pistrol et al., 2023) discussed the relevance of the variable contact geometry between vibrating drum and soil surface and introduced a simple mechanical model that enables the calculation of force-displacement curves that are in good accordance with measurements.

This paper presents a geometric model that allows for the simulation of the variable contact geometry between the drum of a vibratory roller and the soil surface based on measurements from experimental field tests.

2 EXPERIMENTAL FIELD TESTS

The experimental field tests were carried out in a gravel pit near Vienna in 2019 as part of the joint research project between roller manufacturer HAMM AG and the Institute of Geotechnics at TU Wien. The extensive test program is not discussed in this paper but is documented in Hager (2022).

The tests were carried out during an expansion of the gravel pit after the topsoil had been removed. Two test lanes, each 120 m long, were established on the surface of the sandy gravel layer of the gravel pit.

A HAMM H20i single-drum roller was used for the tests. All machine parameters relevant for the ICMV calculation are given in Table 1, additional information can be found in Hager (2022). The particular test referred to in this paper was performed with a large amplitude setting of the roller, an excitation frequency of $f = 25$ Hz and a variation of the travel speed ($v = 2.5 - 4.0 - 6.0$ km/h) along the test lane.

Table 1. Parameters of the HAMM H 20i single-drum roller used in the experimental field tests.

Roller parameter	Value	Unit
Diameter of the drum d	1.60	m
Length of the drum $2a$	2.14	m
Eccentricity e of rotating mass	0.0676	m
Rotating mass m_e	177.4	kg
Mass of the drum m_d	5590.6	kg
Mass of the frame m_f	6807.0	kg

The measuring system consisted of one-dimensional accelerometers with a sensitivity of ±30 g mounted at the bearing of the drum. Accelerations were measured in horizontal direction of travel (x) and in vertical direction (z) with a sampling rate of 10 kHz.

3 FORCE-DISPLACEMENT DIAGRAM BASED ON MEASUREMENTS

A force-displacement diagram can be drawn for each period of excitation utilizing the soil contact force F_b as resulting force

between the drum of the roller and the soil surface, and the vertical displacement s_z of the drum (see Figure 1). The calculation of F_b and the determination of force-displacement diagrams from measurements is extensively documented in the literature (e.g. Kröber, 1988; Adam, 1996; Pistrol et al., 2024).

This kind of diagram is already used for multiple Intelligent Compaction Meter Values (ICMVs) (Anderegg and Kaufmann, 2004; Mooney and Rinehart, 2009) and illustrates the reaction of the soil to the imposed movement of the drum (= resulting system response). The force-displacement relationship enables an analysis of energy, damping and stiffness characteristics for the compacted soil and therefore, provides information for the assessment of numerous compaction parameters.

The points of start and end of contact obtained from the force-displacement diagram (see Figure 1) are of particular interest for this study.

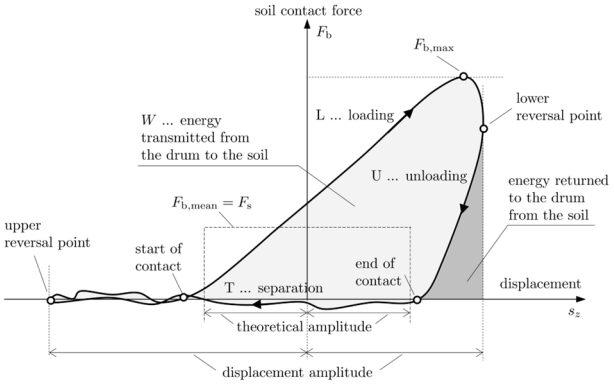

Figure 1. Schematic force-displacement diagram of a vibrating drum (Hager, 2022).

Figure 2 shows the calculated soil contact force F_b from the experimental field tests over the vertical displacements s_z for eight periods of excitation. The diagram is the basis for the calculation of the variable contact area between drum and soil.

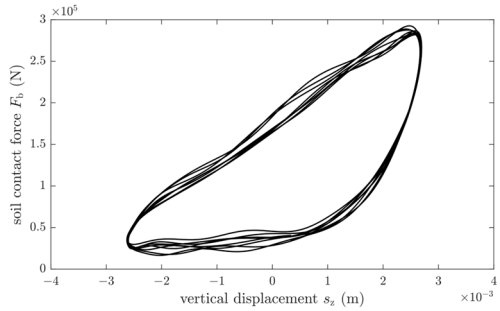

Figure 2. Force-displacement diagram from measurements on the vibrating drum of a HAMM H20i single-drum roller.

4 SIMULATION FOR THE DETERMINATION OF THE CONTACT AREA BETWEEN DRUM AND SOIL

The dynamic interaction between the drum of the roller and the soil is decisively characterized by the contact area between the two subsystems. While the length of the contact area (denoted by $2a$) may be assumed to equal the length of the drum, the contact width (denoted by $2b$) is a variable quantity during the loading phase, due to the cylindrically curved drum and thus causes a significant non-linearity in the interacting system. During the loading phase, the drum increasingly penetrates the soil and the contact width between the two subsystems increases. After the drum reaches the lower reversal point of its motion, the contact width decreases again until it becomes zero and drum and soil move independently of each other during the loss of contact phase.

The simulation presented in the following is based on the measured motion behavior of the drum – considering the points of start and end of contact (see Figure 1) – which is imposed in a path-controlled manner on a simplified geometric model to determine the contact geometry between the drum and the soil (see Figure 3 and Figure 4). The procedure is shown on the example of the "partial uplift" operating mode, as it is the desired mode of operation for compaction work with vibratory rollers. However, the considerations made can be applied analogously to the operating mode "double jump". With respect to the "continuous contact" operating mode, the presented method is limited, since there is no periodic loss of contact, no contact points can be identified, and the contact width remains unknown at any time. However, the operating mode "continuous contact" only plays a minor role in vibratory roller compaction.

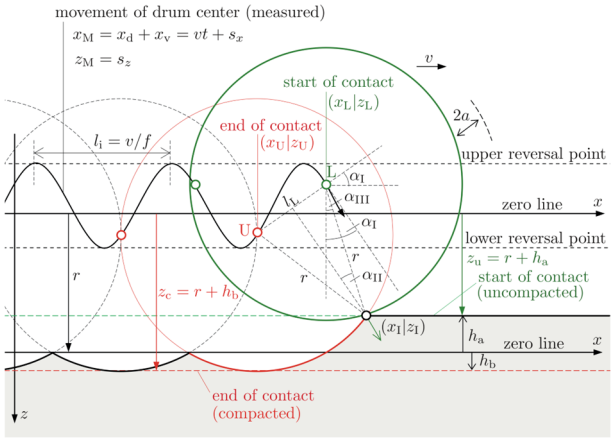

Figure 3. Imposing the measured motion behavior of the drum on a simplified geometric model to determine the contact width $2b$. Illustration for the determination of the input parameters z_u, z_c, h_a, and h_b of the simulation (Pistrol et al., 2024).

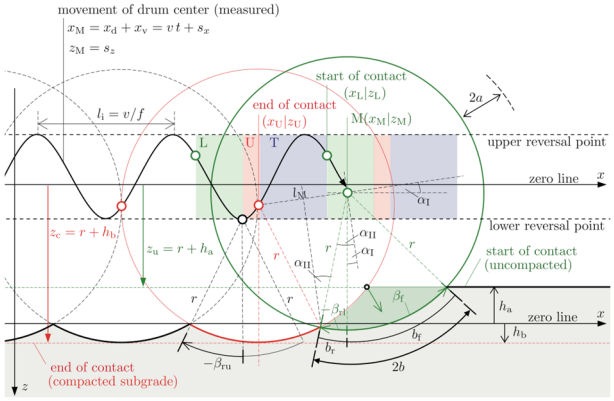

Figure 4. Imposing the measured motion behavior of the drum on a simplified geometric model to determine the contact width 2b. Operating phases: L = loading (green), U = unloading (red), T = separation (blue) (Pistrol et al., 2024).

4.1 *Input parameters of the simulation*

The horizontal and vertical displacements x_M and z_M, respectively, of the drum center M describe the motion behavior of the drum (see Figure 3). The horizontal displacement component x_M comprises the travel distance $x_d = vt$ with speed v and the horizontal component of the vibratory excitation x_v, which equals the displacement s_x calculated from measurements. The vertical displacement component z_M corresponds to the displacement s_z from measurements. The movement of the drum center is thus defined by the

measurements and already contains information about the speed of the roller v, the frequency of the excitation f – and thus also the impact distance $l_i = v/f$ – as well as the direction of rotation of the eccentric mass. The upper and lower reversal points of the drum are given by the amplitude of the vertical drum displacement s_z (see Figure 1 and Figure 3). Note that the geometric relationships in Figure 3 and Figure 4 are not shown to scale – the impact distance l_i and the displacements x_M and z_M are over-scaled compared to the drum radius r.

In the first step, the contact points (start and end of contact) are identified in the force-displacement diagram (see Figure 1) and assigned to the movement of the drum center in Figure 3 resulting in the coordinates of the drum center for the start ($x_L|z_L$) and end ($x_U|z_U$) of contact. It is noted that the determination of these contact points is crucial in the simulation for the determination of the contact area. A mechanically balanced drum with synchronous oscillation (by means of a rigid body movement) is the basis for a sufficient identification of the contact points.

It is assumed that at the end of the unloading phase, i.e. at the time of the end of contact, the drum shape is imprinted in the soil and remains unchanged until the beginning of the next loading phase. From the knowledge of the contact points along the measured drum movement, the essential input parameters for the contact width simulation:

- the level of the subgrade before compaction z_u
- the level of the subgrade after compaction z_c
- the distance h_a of the uncompacted subgrade from the zero line
- the distance h_b of the compacted subgrade from the zero line

can be determined for each period of excitation using geometrical relations (see Figure 3).

At the point of end of contact (drum center coordinates $x_U|z_U$), the drum looses contact to the soil and moves independently until it gets in contact with the soil again at the intersection $x_I|z_I$ of the uncompacted subgrade with the imprinted drum shape of plastic deformations from the previous load cycle at the beginning of the next loading phase (drum center coordinates $x_L|z_L$). The distance l_L between drum center positions at end of contact and start of contact is given by:

$$l_L = \sqrt{(z_U - z_L)^2 + (x_L - x_U)^2} \tag{1}$$

The inclination of distance l_L is defined by the angle α_I:

$$\alpha_I = \tan^{-1}\left(\frac{z_U - z_L}{x_L - x_U}\right) \tag{2}$$

Angle α_{II} (see Figure 4) is:

$$\alpha_{II} = \sin^{-1}\left(\frac{l_L}{2r}\right) \tag{3}$$

where r is the radius of the drum. The difference of the angles α_I and α_{II} is the angle α_{III} between the perpendicular through the center of the drum and the start of the contact at point I which is defined by its coordinates x_I and z_I. The horizontal and vertical distance between the drum center at contact start L and point I are given by:

$$\Delta x = r \sin \alpha_{III} \tag{4}$$

$$\Delta z = r \cos \alpha_{III} \tag{5}$$

The essential input parameters for the subsequent contact width determination in section 4.2 are thus determined. They can be calculated as follows: Distance h_b of the compacted subgrade from the zero line:

$$h_b = z_U \tag{6}$$

Level of the subgrade after compaction z_c:

$$z_c = r + h_b \tag{7}$$

Level of the subgrade before compaction z_u:

$$z_u = z_I = z_L + \Delta z = r + h_a \tag{8}$$

Distance h_a of the uncompacted subgrade from the zero line:

$$h_a = -(r - z_U) \tag{9}$$

The level of the subgrade before compaction z_u (or the vertical distance of the soil surface h_a above the zero line) is significantly influenced by the speed of the roller v, the frequency of the excitation f, the horizontal vibration amplitude s_x and thus by the direction of rotation of the eccentric mass, as well as by the vertical coordinates of the points of start (z_L) and end (z_U) of contact. The level of the subgrade after compaction z_c (or the vertical distance h_b of the compacted subgrade from the zero-line) mainly depends on the coordinates ($x_U|z_U$) of the end of contact point.

4.2 *Determination of the contact width 2b*

At the end of the unloading phase (drum center position U and red in Figure 4), the level of the subgrade after compaction z_c is reached and the drum loses its contact to the soil. These end of contact points ($x_U|z_U$) are obtained from the measurements and it is assumed that the circular drum shape with the center of curvature at ($x_U|z_U$) gets imprinted to the subgrade by means of plastic deformations and remains unchanged until the beginning of the next loading phase. This results in an undulating subgrade after compaction, as shown in Figs. 4 and Figure 4.

After the separation phase (T and blue in Figure 4), in which the two subsystems move independently of each other, and at the beginning of the next load cycle, the drum hits the soil at the intersection of the level of the subgrade before compaction z_u with the imprint of the drum shape from the previous unloading phase (point I in Figure 3) and penetrates into the subgrade again.

The drum with radius r and length 2a (which is assumed to be the length of the contact area) can now be imposed on the soil beginning at the start of contact ($x_L|z_L$) following the measured motion behavior and under consideration of the input parameters z_c, z_u, h_a and h_b obtained in section 4.1. The procedure is shown in Figure 4 for an arbitrary position of the drum center ($x_M|z_M$) during the loading phase and mode of operation ‘‘partial uplift.’’

Analogous to Equations (1) to (3), the distance l_M between the end of contact point and the current drum center position M, its angle of inclination α_I and the angle α_{II} can be computed:

$$l_M = \sqrt{(z_U - z_M)^2 + (x_M - x_U)^2} \tag{10}$$

$$\alpha_I = \tan^{-1}\left(\frac{z_U - z_M}{x_M - x_U}\right) \tag{11}$$

$$\alpha_{II} = \sin^{-1}\left(\frac{l_M}{2r}\right) \tag{12}$$

For every point in time during loading, an angle β_{rl} between the vertical perpendicular through the drum center M and the intersection point of the drum at its current position and the imprinted shape of the previous load cycle is given by:

$$\beta_{rl} = \alpha_I - \alpha_{II} \tag{13}$$

where the sign of β_{rl} is defined by Figure 4.

As soon as the drum reaches its lower reversal point, the drum movement changes from loading to unloading (transition from green (L) to red area (U) in Figure 4). The angle β_{ru} at this point in time between the direct line from the intersection point of the drum and the drum shape from the previous load cycle to the drum center and the vertical perpendicular through the drum center has a negative sign according to Figure 4 and is defined as:

$$\beta_{ru} = -\cos^{-1}\left(\frac{z_c - z_M}{r}\right) \quad (14)$$

The drum subsequently moves upwards and out of the soil again. Therefore, the angle β_{ru} decreases in magnitude until contact is finally lost and the drum contact width $2b$ thus becomes zero.

Both angles, β_{rl} and β_{ru}, describe the rear part of the contact width. Analogous, at every point in time during loading and unloading, an angle β_f can be identified between the vertical perpendicular through the drum center M and the intersection point of drum and subgrade before compaction z_u to define the front part of the contact width:

$$\beta_f = \cos^{-1}\left(\frac{z_u - z_M}{r}\right) \quad (15)$$

The entire contact width $2b$ is the sum of its front part b_f and rear part b_r. It is computed according to Equation (16) under consideration of the definition of sign for the angles in Figure 4:

$$2b = r(\beta_f - \beta_r) \text{ with } \beta_r = \begin{cases} \beta_f & \text{...for T} \\ \beta_{rl} & \text{...for L} \\ \beta_{ru} & \text{...for U} \end{cases} \quad (16)$$

According to Equation (16) the rear part of the contact width b_r is defined in dependence of the operating phase by the angles β_f (separation, T), β_{rl} (loading, L) and β_{ru} (unloading, U), respectively. The front part of the contact width b_f is solely defined by the angle β_f. The maximum contact width is reached at the lower reversal point of the drum, when the operating phase changes from loading to unloading (see Figure 4).

5 RESULTS

The result of the presented simulation is the development of the contact width $2b$ over time. Figure 5 gives an example obtained from the experimental field tests and shows the contact width $2b$ and its components b_f and b_r for the same eight periods of excitation already used in Figure 2.

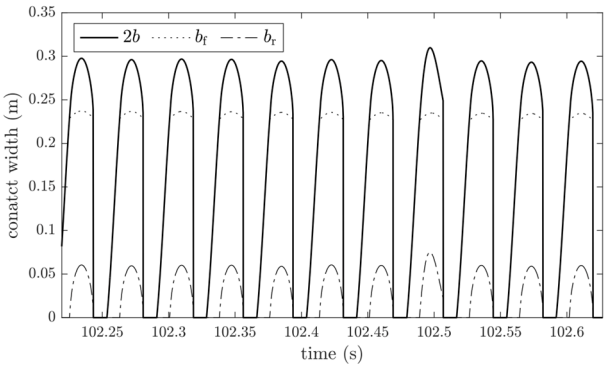

Figure 5. Contact width $2b$ and its components for 8 periods of excitation of the experimental field tests with a HAMM H20i single-drum roller.

The development of the contact width $2b$ for the entire compaction test is shown in Figure 6 which clearly illustrates the influence of the roller speed on the contact width.

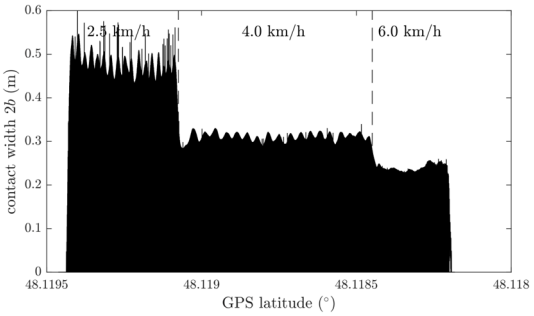

Figure 6. Contact width 2b for the entire length of the test lane of the experimental field tests.

6 CONCLUSIONS

In this paper, a geometric model was presented for the determination of the variable contact geometry between the vibrating drum of a roller and the soil surface based on measurements. The results show a pronounced effect of the roller speed on the size of the contact geometry. The findings of this research may be used for future developments in intelligent compaction.

7 REFERENCES

Adam, D., 1996. *Continuous Compaction Control (CCC) with vibrating rollers (in German)*. PhD Thesis. TU Wien.

Anderegg, R. and Kaufmann, K., 2004. Intelligent Compaction with Vibratory Rollers: Feedback Control Systems in Automatic Compaction and Compaction Control. *Transportation Research Record*, 1868(1), pp.124–134. https://doi.org/10.3141/1868-13.

Cao, Y., Huang, X., Ma, L., Qiu, S. and Gui, S., 2011. Finite element analysis to vibratory drum - Soil model of vibratory roller. [online] Applied Mechanics and Materials. pp.2005–2008. https://doi.org/10.4028/www.scientific.net/AMM.94-96.2005.

Hager, M., 2022. *CCC with Vibrating Rollers -- Development of a new Indicator for Roller-Integrated Continuous Compaction Control (in German)*. PhD Thesis. TU Wien.

Kenneally, B., Musimbi, O.M., Wang, J. and Mooney, M.A., 2015. Finite element analysis of vibratory roller response on layered soil systems. *Computers and Geotechnics*, 67, pp.73–82. https://doi.org/10.1016/j.compgeo.2015.02.015.

Kopf, F., 1998. *Continuous Compaction Control (CCC) during compaction of soil by dynamic rollers with different types of excitation (in German)*. PhD Thesis. TU Wien.

Kröber, W., 1988. *Investigation of the dynamic processes during the vibratory compaction of soils (in German)*. PhD Thesis. Technische Universität München.

Mooney, M.A. and Rinehart, R.V., 2009. In situ soil response to vibratory loading and its relationship to roller-measured soil stiffness. *Journal of Geotechnical and Geoenvironmental Engineering*, 135(8), pp.1022–1031. https://doi.org/10.1061/(ASCE)GT.1943-5606.0000046.

Pistrol, J., Hager, M., Kopf, F. and Adam, D., 2023. Consideration of the Variable Contact Geometry in Vibratory Roller Compaction. *Infrastructures*, 8(7), pp.1–15. https://doi.org/10.3390/infrastructures8070110.

Pistrol, J., Hager, M., Kopf, F. and Adam, D., 2024. An advanced ICMV for vibratory roller compaction. *Acta Geotechnica*, 20(2025), pp.501–517. https://doi.org/10.1007/s11440-024-02342-8.

van Susante, P.J. and Mooney, M.A., 2008. Capturing Nonlinear Vibratory Roller Compactor Behavior through Lumped Parameter Modeling. *Journal of Engineering Mechanics*, 134(8), pp.684–693.

Thurner, H. and Sandström, Å., 1980. A new device for instant compaction control. International Conference of Compaction. Paris, France. pp.611–614.

Yoo, T.-S. and Selig, E.T., 1979. Dynamics of Vibratory-Roller Compaction. *Journal of the Geotechnical Engineering Division*, 105(10), pp.1211–1231. https://doi.org/10.1061/AJGEB6.0000867.